Low-cost system for micrometer-resolution solar cell characterization by light beam-induced current mapping

2014 Meas. Sci. Technol. 25 105801

(http://iopscience.iop.org/0957-0233/25/10/105801)

IOP Publishing Measurement Science and Technology
Meas. Sci. Technol. **25** (2014) 105801 (7pp) doi:10.1088/0957-0233/25/10/105801

Low-cost system for micrometer-resolution solar cell characterization by light beam-induced current mapping

H Cossutta[1], K Taretto[1,2] and M Troviano[1,2]

[1] Departamento de Electrotecnia (FAIN-UNCo), Neuquen, Argentina
[2] Instituto de Investigación y Desarrollo en Ingeniería de Procesos, Biotecnología y Energías Alternativas (PROBIEN, CONICET-UNCo), Neuquen, Argentina

E-mail: kurt.taretto@fain.uncoma.edu.ar

Received 20 February 2014, revised 4 July 2014
Accepted for publication 8 July 2014
Published 29 August 2014

Abstract
Light-beam induced current (LBIC) mapping is an increasingly utilized characterization technique for laboratory-scale as well as industrial-scale solar cells, which measures the local solar cell photocurrent by point illumination. This contribution demonstrates the design and testing of an LBIC mapping device capable of measuring LBIC maps of solar cells using inexpensive materials. With a spatial resolution of 4 μm and an auto-focused beam spot size of about 2 μm, obtained from a standard CD/DVD pickup, high-resolution LBIC maps of thin-film solar cells are obtained. The system was demonstrated by measuring LBIC maps on thin-film solar cells, revealing significant, micrometer-sized photocurrent heterogeneities that are otherwise unseen when using typical commercial LBIC systems with lower resolution.

Keywords: solar cell, photocurrent mapping, light beam-induced current, LBIC, laser pickup, S-curve, CD-DVD

(Some figures may appear in colour only in the online journal)

1. Introduction

Solar-cell efficiency is strongly controlled by the homogeneity of the local photovoltaic response over the area of a given solar cell. Therefore, characterization methods that scan the local response of a solar cell across its area are fundamental for optimizing preparation processes and materials. When the solar cell is locally excited by a narrow light beam, the measurement of the photocurrent delivered by the cell as a function of the position on the cell is known as the light beam-induced current (LBIC) method. LBIC measurements deliver two-dimensional photocurrent data (LBIC maps) showing the variations of photocurrent across the extension of the sample solar cell [1]. This method has been widely applied in industry [2] and among the scientific community to reveal several defect types, e.g. cracks in crystalline solar cells (mechanical defects) [3], crystal dislocations [4] and grain boundaries (crystalline defects) [5, 6], detrimental crystal orientations [7], chemical heterogeneities that arise during processing [8, 9], and fabrication defects such as shunts [10]. The technique is not only applied to conventional wafer-based solar cells [11], but also to state-of-the-art inorganic [12] and organic thin-film solar cells at the laboratory [9, 13] and pilot plant scale [14]. Furthermore, LBIC has been recently applied to assess the effectiveness of light-trapping structures in advanced solar-cell designs [15].

A small number of LBIC systems are commercially available [16, 17]; the spatial resolution of such systems is 50 μm to 100 μm. Although these values are sufficient to respond to the technical demands of industrial-testing facilities, higher resolution is often required on the scientific laboratory scale to differentiate defect types and, in combination with other characterization techniques, correlate photocurrent heterogeneities with the preparation techniques. Higher-resolution LBIC mapping systems are occasionally constructed for specific, low-throughput laboratory-scale investigations [5, 18]. Such systems achieve very high accuracy and resolution, but generally require expensive optical and electromechanical parts.

This contribution proposes an LBIC system with a resolution up to 4 μm that can be constructed using inexpensive materials. The key to accomplish this goal is adapting a compact/digital versatile disc (CD/DVD) laser module. Such adaptations performed successfully in several other applications, e.g. cantilever displacement sensing for atomic force microscopy [19] and topographic profile measurement [20]. Here, we design a driver circuit that allows auto-focusing and operating of the CD/DVD module on low-reflectance objects such as solar cells. The paper goes through the different design stages of the LBIC system, including the required optics, mechanics and computer interfaces. The approach is to show how the whole measurement system is understood in conjunction with several sub-systems, which are described separately. We explain the strategies followed in the key electronic circuits, leaving some parts that are directly adapted from more conventional electronics solutions to the reader. This work is aimed at scientists and technicians from the field of experimental photovoltaics, as well as custom electronic photodetection or digital imaging.

2. Set-up design

2.1. Overview

Figure 1 shows a schematic diagram of the complete system containing the most important components and the connections between them. At the bottom of the diagram we find the solar cell to be mapped, which is illuminated locally by a laser light beam emitted by a CD/DVD laser pickup. A transimpedance amplifier with gain G measures the photocurrent I delivered by the solar cell, transmitting a proportional voltage V to the programmable integrated circuit (PIC) on the mainboard, seen at the top of the diagram. The mainboard communicates with a laptop through a standard serial bus. The laser diode light output and autofocus (AF) are controlled by a circuit board that communicates with the laptop separately through universal serial bus (USB). The CD/DVD pickup is positioned over the solar cell by an x–y stage using stepper motors, which are driven by the PIC, enabling an x–y scanning sequence to scan the desired solar-cell area. When the autofocus state is reached, the AF control sends a flag to the mainboard, enabling the acquisition of the cells' signal and the movement of the pickup to the next position.

2.2. Laser driver and autofocus

As light beam source, a regular audio/video CD/DVD pickup model SF-HD65 is chosen [21], which is driven by an in-house designed control board. The pickup allows choosing between CD (780 nm) and DVD (650 nm) light wavelength; LBIC scanning can be performed in these two wavelengths. The pickups' laser diode (LD) power output is controlled using the signal from the monitor photodiode integrated into the LD casing and an analog power-control circuit (APC) that follows the design proposed in [21]. The light output power of the pickup is measured by illuminating a calibrated silicon cell (external quantum efficiency of 0.71 at 650 nm) with the pickup, yielding 0.377 mW. This value is in the nominal range of 0.31 mW to 0.70 mW provided by the data sheet [21].

The vertical movement of the lens is performed using the coil attached to the lens of the pickup, which is driven by the circuit shown in figure 2. The coil is biased using two power OP-AMPs that provide voltages from –1 to +1 V between the extremes of the coil, resulting in 1 mm as the total excursion of the lens. The OP-AMP's input is generated by active, 2nd-order low pass filters (LPF) of pulse-width modulation signals (PWM) generated on the AF- and LD-control board by a 18F550 PIC. The combination of the PWM and the active filters allows the lens height to be established with a resolution of 2048 steps, implying a displacement resolution of 0.49 μm/step. The lens position corresponding to the focused state is chosen by the PIC, as explained below. The 'degree of focus' is measured by the S-curve obtained from four photodiodes within the pickup [20], which receive the light reflected by the illuminated surface—i.e. the sample or solar cell, as seen through the lens. (For a better understanding of autofocusing by the S-curve method, see [22, 23].) The S-curve value is obtained by analogically calculating the value (A+B)–(C+D), in which each letter corresponds to the photocurrent delivered by each of the photodiodes. In order to find the focus position, the lens is moved from the top to the bottom of its excursion until the position corresponding with the center of the S-curve is found, relating to the focused state.

The calculated value of the S-curve is amplified by an integrated AD620 instrumentation amplifier. Since solar cells may differ strongly in their reflectance depending on technology, material and encapsulation, the amplifier's circuit is designed with selectable gain through different combinations of gain resistors, enabling acquisition of S-curves even on extremely low-reflectance surfaces. Figure 3 shows S-curves measured on three different objects: the first corresponds to a compact disc, the second to a silicon solar cell, and the third to a thin-film $CuInGaSe_2$ (or CIGS) solar cell. Next to each curve we find in parentheses the gain utilized in each case, the CD requiring much lower gain than the solar cells according to its much higher reflectance. Further, the horizontal scale bar indicates that the S-curves are contained in a narrow range smaller than 100 μm. It can also be shown that the focused state, corresponding to the central part of the curve, spans approximately 10 μm.

2.3. Photocurrent measurement

The photocurrent delivered by the illuminated solar cell is also measured using an AD620, with a selectable gain between 5 and 400. This amplifier is effectively working as a transimpedance amplifier, using an input resistance that enables the solar cell to work as a current source. In order to satisfy near-short-circuit conditions, the value of the input resistance must be much smaller than the cell's internal shunt resistance. In the cells studied here, the shunt resistance was higher than 1500 Ω and therefore an input resistance of 10 Ω was chosen. The signal levels are adapted to the input of a

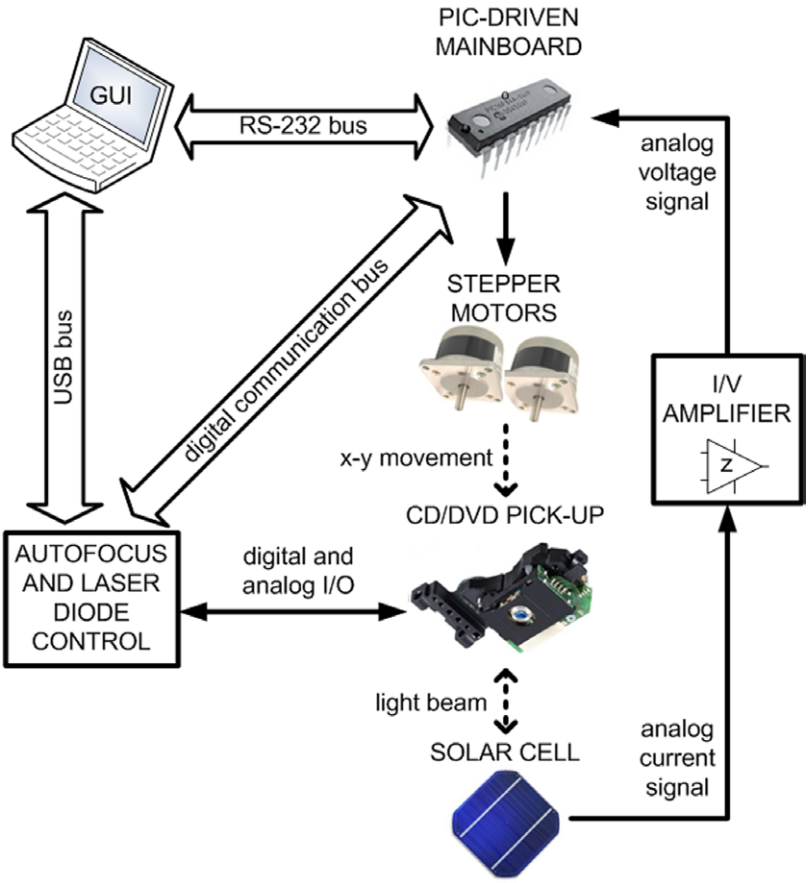

Figure 1. Schematic diagram of the designed LBIC measuring system. The solar cell, placed at the bottom of the diagram, is illuminated by a small spot of light emitted by the CD/DVD pick-up, which is placed over the solar cell on a specific x–y position established by a stepping motor mechanism, controlled by the mainboard (top). The focus and light power of the laser spot is controlled by a circuit (lower left) which communicates with the computer as well as the mainboard.

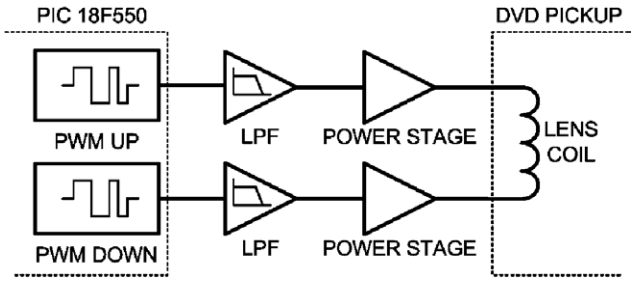

Figure 2. Circuit implemented for the movement of the lens in the pick-up. The lens is attached to a coil surrounded by a permanent magnet fixed to the pick-up. The precise polarization of the coil enables to adjust the position of the lens by 0.49 μm per step of the pulsed width modulation (PWM) delivered by the PIC.

10-bit analog-to-digital (A/D) converter integrated into the mainboard's PIC microcontroller. The output of the AD620 transimpedance amplifier is buffered by an OP-AMP as a protection element for the microcontroller. In order to calibrate the current measurement, we measured the response of the A/D converter as a function of the input current by injecting precisely known currents with a Keithley 2400 source meter, which was able to digitally set current values with an accuracy of 0.0045%. The output of the A/D converter in counts C is shown as a function of the input current I in figure 4 (circles).

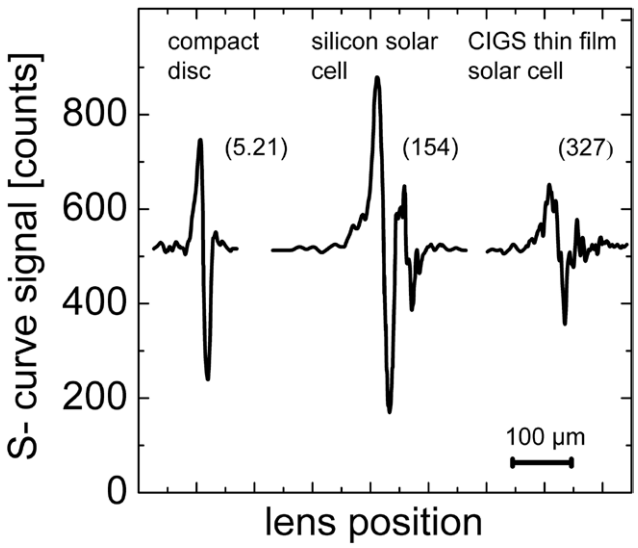

Figure 3. S-curves obtained on a CD surface (left curve), a silicon solar cell (center) and on a thin film CIGS solar cell (right). The numbers in parentheses next to each curve indicated the gain factor require d in each case. The horizontal scale bar (bottom right) shows that the S-curves are found in a range below 100 μm.

At each current value we probed 200 measurements, and since for a given I the dispersion between values is very low,

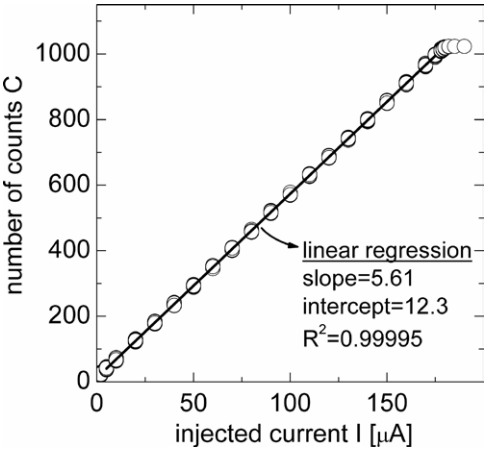

Figure 4. Digitalized output in counts C (circles) of the transimpedance amplifier AD620 (center right in figure 1) as a function of the injected current I, measured 200 times at each injected current value. The straight line is a linear regression that serves as calibration line for the current measurements.

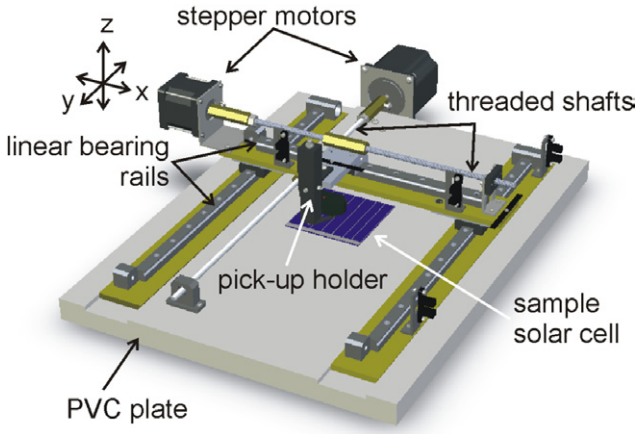

Figure 5. Schematic view of the 2-axis positioning stage. This positioning system moves the CD/DVD pickup in the x and y directions using linear bearing precision rails that are mounted in an H-shape geometry. The movement is given by stepping motors and threaded shafts attached to each carriage.

most data circles overlap and are not appreciated in the figure. The expected linearity between injected current and counts appears between 3 μA and 175 μA, where we performed a linear regression analysis (solid line in figure 4) to obtain the calibration line for the photocurrent. The R-square factor corresponding to this fit is 0.99995.

Further, the stability of the current measurement was probed, performing 250 000 measurements of an injected current I = 50 μA, taking about 2 h of continuous sensing. This resulted in no appreciable increase or decrease of the measured values and a statistical deviation of 0.8%.

During standard measurement conditions, random measurement errors are filtered out by digitally averaging over 20 photocurrent measurements, calculating the standard variation and the mean value. If the standard deviation relative to the mean value exceeds 0.1%, a new measurement attempt of 20 samples is performed until the 0.1% criterion is satisfied. The resulting mean value of the photocurrent is stored and sent to the computer, together with the x–y values.

2.4. x–y translation stage

The designed x–y stage is capable of moving the CD/DVD pickup on an area of 12 cm × 19 cm, which is suited for both small-scale laboratory solar cells and larger, industrial-scale cells or minimodules. As shown in figure 5, the stage consists of three linear bearing rails mounted on a high-molecular-weight polyethylene plate. Two linear bearing rails attached to the plate run parallel along the y-direction, while the third rail is mounted on the carriages of the y-axis rails, forming an H-shaped geometry (see figure 5). Both lower rails provide movement to the upper rail in the y direction, while the upper rail provides movement in the x direction. The movement of each stage is achieved by stepper motors and threaded shafts. The motors transmit the movement to the shafts using helicoidal shaft-couplers, which allow for small, angular misalignments and zero backlash. The threaded shafts allow for a minimum displacement of 2 μm/step. This is smaller than the size of the CD laser spot, which typically is about 2.55 μm in diameter when correctly focused [22], corresponding to the $\pm 3\sigma$ width of a Gaussian distribution for the intensity of the beam. (At the DVD wavelength, the spot width is 1.65 μm.) Although 2.55 μm is a good approximation for the spot diameter in CD mode, the exact spot size may be larger in practice since it depends on the final lens position chosen by the autofocusing algorithm, which can vary from sample (or surface) to sample. Thus, in order to ensure that the steps are slightly larger than the spot size and avoid overlaps, we assume that the highest resolution of the LBIC set-up is 4 μm. Further, since the spot size is given by the focus, it is always chosen independently of the step size chosen for displacements.

The measurement speed of the set-up is directly proportional to the area to be scanned, and inversely proportional to the step size squared. Our measurements show that on a scanning area of e.g. 1000 μm × 1000 μm using 10 μm steps (i.e. 10 201 points), the measurement takes 5 min, while 4 μm steps (i.e. 63 001 points) need about 30 min. For routine LBIC measurements of large samples such as industrial silicon solar cells, possible time-saving strategies could be statistical sampling of different locations of a solar cell, and the use of large step sizes to find possible areas of interest.

3. Sample measurement results

The LBIC apparatus was tested on laboratory-scale thin-film solar cells prepared at the Institut für Photovolaik (IPV) at Stuttgart University, Germany [24]. This thin-film solar cell is composed of several layers of different materials deposited by physical vapor deposition, chemical bath deposition and sputtering. The photovoltaically active material is the quaternary semiconductor $CuInGaSe_2$, or CIGS. Current CIGS solar cells deliver the highest energy conversion efficiencies from all thin-film solar cells, with a record of 20.4% in laboratory-scale devices [25]. Despite

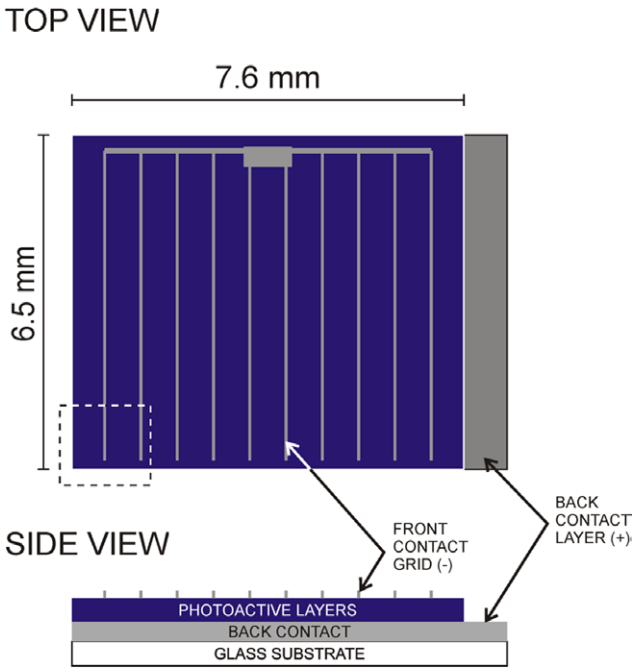

Figure 6. Dimensions and features of the thin film CIGS solar cell, showing the front contact grid and the back contact layer. The dashed box in the lower left corner of the top view shows the area chosen for the LBIC mapping.

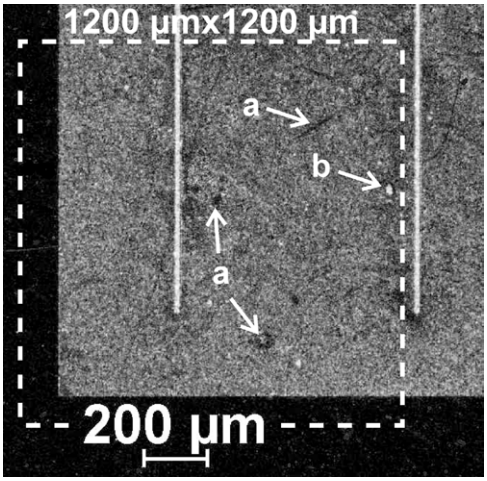

Figure 7. Photograph of the lower left corner of the investigated solar cell, showing two contact fingers seen as white vertical lines. The dashed box represents the area chosen for LBIC scanning. Several defects are marked with letters **a** and **b**, to be compared with the LBIC images in figure 8.

such remarkable results, it has become clear among the scientific community related to CIGS that the efficiency can only be improved if more material knowledge and deposition control are achieved. A key factor on the path to higher efficiencies is the homogeneity of the involved layers, since heterogeneous electronic properties of the layers lead to photogeneration losses [26, 27].

The tested CIGS solar cell is schematically shown in figure 6, of which the top view shows the dimensions of the device and displays the top metal grid, which serves as an electron-collecting contact (i.e. negative contact), as well as the back contact on the right side of the cell. The dotted box in the bottom-left part of the cell corresponds to the area chosen to perform LBIC scans shown below. The side view (bottom of figure 6) reveals that the back contact covers the whole back surface of the solar cell, serving as a uniform hole collecting contact (i.e. positive contact). Notice that this thin-film solar cell is deposited on a mechanically supporting substrate (typically glass), since the active layers are only about 3 μm thick in total. The layer thicknesses are not to scale.

Figure 7 shows a photograph taken with a microscope at fourfold magnification, corresponding to the bottom-left part of the cell, according to the top view of figure 6. The white vertical lines are two contacting fingers (cf. figure 6), which are obtained by aluminum shadow-mask evaporation. The fine granular aspect of the cell surface is attributed to surface roughness, while more localized defects (such as the ones marked with **a** and **b**) may correspond with production defects as well as post-production handling. Using a magnification of 40 × (not shown here), a width of 10 μm of the contact finger was measured, showing fluctuations below 1 μm along the observed length. The dotted box in figure 7 covers an area of 1200 μm × 1200 μm, where the LBIC mapping was performed. (See below.)

Figure 8(*a*) and (*b*) show the measured LBIC map at 650 nm (DVD mode), corresponding with the dotted area in figure 7—obtained using 10 μm and 4 μm steps, respectively. The color scale goes from black (60% of the maximum photocurrent in the measurement, 102 μA) through cold colors to warmer colors, with deep red representing the maximum photocurrent. The higher resolution of LBIC map B is clearly seen around the contact finger, which appears much more refined compared with map A. Both maps reveal point heterogeneities, i.e. dark spots (in which dark means low photocurrent, i.e. black or cold-colored spots in figure 8), and several diagonal, segment-shaped spots most clearly seen around the center of each image. Interestingly, these defects are not seen in the photograph of figure 7, indicating that the measured defects do not correspond to surface defects that deliver higher reflectance, but to electronic defects within the active layer of the solar cell. This opens the path for further investigations aimed at determining the nature of the observed defects, e.g. whether they are of chemical or physical nature, or if they originated during or after cell preparation. Moreover, only defect **b**, seen in the photograph of figure 7, also appears on the LBIC maps; defects **a** are not seen. Defect **b** is related to light reflectance, since it is seen as a white spot in figure 7, possibly generated by a surface-adhered particle.

Notice that most of the observed dark spots and lines in the LBIC maps are smaller than 50 μm, which are appreciated with sufficient detail using the chosen high resolutions of 10 μm or 4 μm. This means that typical commercial LBIC characterization equipment with resolution between 50 μm and 200 μm would not reveal these defects appropriately. And, most evidently, the 10 μm wide contact fingers require a step resolution below 10 μm to be resolved appropriately.

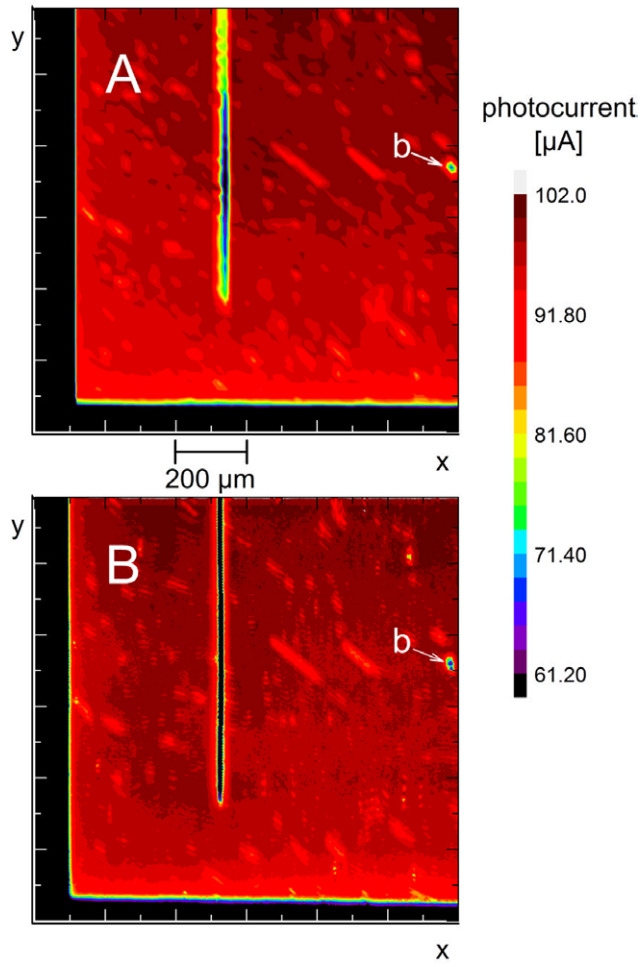

Figure 8. Light-beam induced current (LBIC) maps of the area shown in figure 7 (dotted line) of a thin-film CIGS solar cell. The color scale goes from black through cold colors to warmer colors, where dark red represents the maximum photocurrent of 102 μA. Map A was measured with 10 μm steps in x and y directions, while map B uses 4 μm steps in both directions. The higher resolution of map B allows resolving the 10 μm-wide contact finger (vertical black line) with sufficient precision. See text for further discussion.

4. Conclusions

A low-cost, high-resolution light beam-induced current (LBIC) measurement system was developed using conventional electronic parts, the main component being a CD/DVD laser pick-up module mounted on an in-house designed x–y stage, providing a high movement resolution of up to 4 μm. The small light spot (about 2 μm diameter) required to achieve highly resolved LBIC maps is obtained by autofocusing the laser light with the pickup's internal photodiode array and the S-curve method. We developed the corresponding circuits for the whole system: laser diode drivers, x–y movement stage, photodetector array and autofocusing electronics, solar-cell photocurrent detection, and PC-communication systems. All circuit schematics are available upon request to the authors by personal communication.

The system was tested measuring LBIC maps of high-efficiency $CuInGaSe_2$ thin-film solar cells, revealing several defects that point to heterogeneous fabrication. The revealed defects suggest a path towards higher solar-cell efficiency through higher film homogeneity. These defects were made visible by the high spatial resolution of measurement, which typical commercial-grade LBIC systems are not able to resolve. Future studies will include scans in both CD and DVD wavelengths, establishing comparisons between both LBIC maps.

A possible further improvement to the system is the measurement of the light reflectance of the cell by computing the reflected light, which may be readily available from the pickup photodiodes signal.

References

[1] Goetzberger A, Knobloch J, Voss B and Waddington R 1998 *Crystalline Silicon Solar Cells* (Chichester: Wiley)

[2] Acciarri M, Binetti S, Racz A, Pizzini S and Agostinelli G 2002 Fast LBIC in-line characterization for process quality control in the photovoltaic industry *Sol. Energy Mater. Sol. Cells* **72** 417–24

[3] Kaminski A, Breitenstein O, Boyeaux J P, Rakotoniaina P and Laugier A 2004 Light beam induced current and infrared thermography studies of multicrystalline silicon solar cells *J. Phys. Condens. Matter* **16** S9

[4] Mariani J L, Pichaud B, Minari F and Martinuzzi S 1989 LBIC measurements of the recombining activity of dislocations in float zone silicon *Mater. Sci. Eng.* B **4** 347–52

[5] Jellison G E, Budai J D, Bennett C J C, Tischler J Z, Duty C E, Yelundur V and Rohatgi A 2010 High-resolution x-ray and light beam induced current (LBIC) measurements of multicrystalline silicon solar cells *PVSC: 2010 35th IEEE Photovoltaic Specialists Conference* pp 001715–20

[6] Marek J 1984 Light-beam-induced current characterization of grain boundaries *J. Appl. Phys.* **55** 318–26

[7] Wagner T A, Oberbeck L, Nerding M, Strunk H P and Bergmann R B 2001 Orientation-dependence of low temperature epitaxial silicon growth *MRS Proceedings* vol 664 (Boston, MA: Cambridge University Press)

[8] Ostrowski D P, Glaz M S, Goodfellow B W, Akhavan V A, Panthani M G, Korgel B A and Vanden Bout D A 2010 Mapping spatial heterogeneity in $Cu(In_{1-x}Ga_x)Se_2$ nanocrystal-based photovoltaics with scanning photocurrent and fluorescence microscopy *Small* **6** 2832–6

[9] Krebs F C, Søndergaard R and Jørgensen M 2011 Printed metal back electrodes for R2R fabricated polymer solar cells studied using the LBIC technique *Sol. Energy Mater. Sol. Cells* **95** 1348–53

[10] Vorasayan P, Betts T R, Tiwari A N and Gottschalg R 2009 Multi-laser LBIC system for thin film PV module characterisation *Sol. Energy Mater. Sol. Cells* **93** 917–21

[11] Martinuzzi S and Stemmer M 1994 Mapping of defects and their recombination strenght by a light-beam-induced current in silicon wafers *Mater. Sci. Eng.* B **24** 152–8

[12] Swanson D E, Geisthardt R M, McGoffin J T, Williams J D and Sites J R 2013 Improved CdTe solar-cell performance by plasma cleaning the TCO layer *IEEE J. Photovolt.* **3** 838–42

[13] Feron K, Nagle T J, Rozanski L J, Gong B B and Fell C J 2013 Spatially resolved photocurrent measurements of organic solar cells: tracking water ingress at edges and pinholes *Sol. Energy Mater. Sol. Cells* **109** 169–77

[14] Krebs F C, Søndergaard R and Jørgensen M 2011 Printed metal back electrodes for R2R fabricated polymer solar cells studied using the LBIC technique *Sol. Energy Mater. Sol. Cells* **95** 1348–53

[15] Schneider J, Turek M, Dyrba M, Baumann I, Koll B and Booz T 2014 Combined effect of light harvesting strings, anti-reflective coating, thin glass, and high ultraviolet transmission encapsulant to reduce optical losses in solar modules *Prog. Photovolt. Res. Appl.* **22** 830–7
[16] PV Tools GmbH (Germany), http://www.pv-tools.de/products/loana-system/methods/lbic.html (accessed 19 Febuary 2014)
[17] Semilab Semiconductor Physics Laboratory Co. Ltd. (Hungary), http://www.semilab.hu/technologies/pvi/light-beam-induced-current (accessed 19 Feburay 2014)
[18] Leite M S, Abashin M, Lezec H J, Gianfrancesco A G, Talin A A and Zhitenev N B 2014 Mapping the local photoelectronic properties of polycrystalline solar cells through high resolution laser-beam-induced current microscopy *IEEE J. Photovolt.* **4** 311–6
[19] Hwu E-T, Huang K-Y, Hung S-K and Hwang I-S 2006 Measurement of cantilever displacement using a compact disk/digital versatile disk pickup head *Jpn. J. Appl. Phys.* **45** 2368
[20] Fan K-C, Chu C-L and Mou J-I 2001 Development of a low-cost autofocusing probe for profile measurement *Meas. Sci. Technol.* **12** 2137
[21] Optical Business-Systems Business Unit 2006 Optical DVD pick-up—Specifications—Model: SF-HD65
[22] Bass M and Optical Society of America 1995 *Handbook of Optics* (New York: McGraw-Hill) p 31.13
[23] Watkinson J 2002 *An Introduction to Digital Audio* (Oxford: Focal) p 378
[24] Jackson P, Würz R, Rau U, Mattheis J, Kurth M, Schlötzer T, Bilger G and Werner J H 2007 High quality baseline for high efficiency $Cu(In_{1-x}Ga_x)Se_2$ Solar Cells *Prog. Photovolt. Res. Appl.* **15** 507–19
[25] Green M A, Emery K, Hishikawa Y, Warta W and Dunlop E D 2013 Solar cell efficiency tables (version 42) *Prog. Photovolt. Res. Appl.* **21** 827–37
[26] Werner J H, Mattheis J and Rau U 2005 Efficiency limitations of polycrystalline thin film solar cells: case of $Cu(In,Ga)Se_2$ *Thin Solid Films* **480–481** 399–409
[27] Haarstrich J, Metzner H, Oertel M, Ronning C, Rissom T, Kaufmann C A, Unold T, Schock H W, Windeln J, Mannstadt W and Rudigier-Voigt E 2011 Increased homogeneity and open-circuit voltage of $Cu(In,Ga)Se_2$ solar cells due to higher deposition temperature *Sol. Energy Mater. Sol. Cells* **95** 1028–30